Sustainable Chemistry for the Environment 5 (2024) 100071

Contents lists available at ScienceDirect

Sustainable Chemistry for the Environment

journal homepage: www.editorialmanager.com/scenv

Designing sustainable porous graphene-$CaTiO_3$ nanocomposite for environmental remediation

D. Krishna Bhat [a,*], Harsha Bantawal [a], P.I. Uma [a], S. Pavan Kumar [a], U. Sandhya Shenoy [b,*]

[a] Department of Chemistry, National Institute of Technology Karnataka, Surathkal, Mangalore 575025, India
[b] Department of Materials Science and Engineering, Institute of Engineering and Technology, Srinivas University, Mukka, Mangalore 574146, India

ARTICLE INFO

Keywords:
Porous graphene nanocomposite
Calcium titanate
Photocatalysis
Density functional theory
Methylene blue dye degradation

ABSTRACT

In the pursuit of sustainable energy and environmental solutions, photocatalysis has emerged as a transformative technology, harnessing the power of light to drive chemical transformations. Among the myriad photocatalytic materials, calcium titanate ($CaTiO_3$) stands out as a promising candidate, holding the potential to revolutionize the landscape of photocatalysis. To further improvise the efficiency of $CaTiO_3$ in this work, porous graphene-$CaTiO_3$ nanocomposite was synthesized by a straightforward solvothermal method and its photocatalytic activity was tested for the degradation of methylene blue dye under visible light. The synthesized sample exhibited 98.1% degradation in 40 min with excellent cyclic stability. Experimental and computational analysis attributed the enhanced performance to the strong chemical interaction of $CaTiO_3$ cuboids with PG sheets via Ti-O-C bond which led to efficient electron hole separation leading to enhanced lifetime of the charge carriers. This along with reduced band gap and increased surface area made the material a potent photocatalyst for the degradation of dyes in short duration.

1. Introduction

The present situation of our world is daunting due to rapid industrial development and high population density which has caused severe damage to the planet especially to the water bodies which harms both human beings and aquatic life. This has necessitated research to find solutions for environmental remediation. Photocatalysis is an ideal green technology for the removal of harmful pollutants in water that employs natural sunlight as a renewable energy source under ambient operating conditions [1,2]. In this connection, many materials have been used as photocatalysts in the past, among which oxides have been the most widely used due to their non-toxicity, low cost, and long-term stability [3,4]. Perovskite-based metal oxides that include vanadates, titanates, and tungstates, have been extensively researched as multi-functional materials with applications in photocatalysis and thermo-electrics [5–11]. Among various perovskite titanates, $CaTiO_3$ has been found to be the attractive candidate in the field of photocatalysis for the degradation of harmful organic pollutants and water splitting [12–14]. However, large band gap and rapid charge recombination are the most dreadful concerns that should be resolved to enhance photocatalytic efficiency [15]. Compositing with 2D materials and doping with metallic or non-metallic ions are the most promising strategies employed to improve photocatalytic efficiency [14,16–18]. Doping is known to be an effective technique for the augmentation of visible light response of wide band gap photocatalyst but on the other hand, it is also known to introduce undesirable in-gap states which function as recombination centers, thus limiting the photocatalytic efficiency of the material [19,20]. In addition, weak carrier transport results in a suppressed lifetime of photogenerated charges. As a result, coupling $CaTiO_3$ with an efficient conducting support is necessary to enable the rapid delivery of charge carriers to the reaction site.

Graphene, a two-dimensional sheet-like material consisting of sp^2 hybridized carbon atoms arranged in a hexagonal pattern, demonstrates some exciting properties like excellent electrical conductivity, thermal conductivity, optical transparency, mechanical strength, and chemical stability [21]. Porous graphene (PG), which is obtained by the removal of some sp^2 hybrid carbon atoms is known to possess all the properties of graphene and in addition to this has a highly porous structure and a very high surface area [16,22–24]. The review of literature revealed that there were a few reports of compositing $CaTiO_3$ with graphene to obtain improved properties. Kumar et al. reported nitrogen-doped $CaTiO_3$-reduced graphene oxide composite for the photocatalytic degradation of

* Corresponding authors.
E-mail addresses: denthajekb@gmail.com (D.K. Bhat), sandhyashenoy347@gmail.com (U.S. Shenoy).

https://doi.org/10.1016/j.scenv.2024.100071
Received 20 June 2023; Received in revised form 8 January 2024; Accepted 8 January 2024
Available online 11 January 2024

methylene blue (MB). The improved activity (95% in 180 min) under visible light was ascribed to the excellent adsorption capacity and suppressed charge recombination [25]. Xian et al. reported 98% photocatalytic degradation of methyl orange in 60 min by $CaTiO_3$-graphene composite under UV irradiation due to the effective suppression of photoinduced charges [26]. Further, we found that there have been no reports devoted to the synthesis and photocatalytic activity of porous graphene-$CaTiO_3$ (PGC) composite. Recently we had investigated the photocatalytic property of PG wrapped $SrTiO_3$ and $BaTiO_3$ nanocomposite for the degradation of MB [16,27]. The excellent photocatalytic efficiency (~92% in 120 min and 98.6% in 80 min for PG-$SrTiO_3$ and PG-$BaTiO_3$ composites, respectively) was attributed to the high surface area, efficient absorption of visible light and enhanced lifetime of photoinduced charge carriers [16,27]. Motivated by these results, we were interested in investigating the photocatalytic property of PGC composite.

Herein, we have synthesized PGC composite by employing a solvothermal approach. The synthesized materials were carefully analyzed by various advanced characterization techniques to obtain information on the purity, crystal structure, morphology, elemental oxidation states and optical properties. MB dye was considered as a model pollutant for the determination of the photocatalytic activity of the synthesized composite materials. The outstanding photocatalytic activity (98.1% degradation in 40 min) of the composite was attributed to the high adsorption capacity of the composite, enhanced photoabsorption in the visible region of the solar spectrum and rapid transport of photogenerated charges via Ti-O-C bonds increasing the lifetime of carriers. Hence, the work not only contributes to the fundamental understanding of photocatalysis process in PGC but also holds the promise of addressing pressing global challenges by paving way for future advancements in environmental remediation.

2. Method

2.1. Preparation of PGC composite

All the chemicals were purchased from Sigma-Aldrich and were used as received. $CaTiO_3$ and GO were produced according to the previously reported method [14,24]. 'x PGC' (x = 2.5, 5.0, 7.5, 10.0 and 12.5 wt% GO) was prepared by a straightforward solvothermal approach as follows: An intended amount of $CaTiO_3$ powder was stirred in a solution of 1:1 water-ethylene glycol mixture containing dispersed GO to obtain a brownish white suspension. The resultant suspension was sealed in an autoclave and kept at 160 °C for 16 h. The black precipitates formed were carefully washed with distilled water and dried in an oven at 70 °C for 8 h. The obtained composite by taking 2.5, 5.0, 7.5, 10.0, and 12.5 wt % GO was labelled 2.5 PGC, 5.0 PGC, 7.5 PGC, 10 PGC, and 12.5 PGC, respectively.

2.2. Characterization

The powder X-ray diffraction (XRD) study of the synthesized samples was performed by using a Rigaku Miniflex 600 diffractometer equipped with monochromatic Cu-K_α radiation ($\lambda = 0.154$ nm) at a scan rate of 2° per minute in the range of 25°–80°. Raman spectra was recorded using a diode pumped solid state laser operating at 532 nm (Renishaw Invia). X-ray photoelectron spectroscopy (XPS) measurement was performed with the help of a Kratos XSAM800 spectrometer equipped with an Al K_α source. The morphological features of the synthesized materials were analyzed using field emission scanning electron microscopy (FESEM, Carl Zeiss Ultra 55) and transmission electron microscope (TEM, Fie Tecnai G2). Nitrogen adsorption-desorption isotherms were obtained using a BEL SORP II, JAPAN at 77 K. The specific surface areas were determined by Brunauer–Emmett–Teller (BET) method and the pore size distributions were determined by using the Barrett-Joyner-Halenda (BJH) method. Diffuse reflectance (DR) spectra were recorded using a UV–visible DR spectrometer (DRS, DR SPECORD S600 Analytic Jena) and the photoluminescence (PL) spectra were recorded using 310 nm excitation wavelength (LS-55, Perkin Elmer Instruments) at room temperature.

2.3. First principles calculations

Density of states (DOS) calculations of $CaTiO_3$, PG and PGC were carried out using Quantum ESPRESSO package within the framework of density functional theory (DFT) [28]. Ultrasoft Perdew, Burke and Ernzerhof (PBE) pseudopotentials implementing generalized gradient approximation was used for the simulations [29]. 4 s^2 of Ca, $3d^2 4\ s^2$ of Ti, 2 $s^2 2p^4$ of O and 2 $s^2 2p^2$ of C were considered as valence electrons. Fully relaxed 5 × 5 × 1 supercell of PG with orthorhombic $CaTiO_3$ cluster and a vacuum of 12 Å in z direction to avoid interaction between the composite layers were used for the simulations. Brillouin zone integrations were sampled using a k-mesh of 9 × 9 × 1 for scf and denser mesh of 18 × 18 × 1 for nscf calculations. The plane wave basis representing the wavefunctions were terminated with an energy cutoff of 50 Ry and charge density cutoff of 400 Ry.

2.4. Determination of photocatalytic activity

To 50 mL of MB solution (10 ppm), 50 mg of the synthesized catalyst was added and dispersed with the help of a sonicator for 5 min. The resultant suspension taken in a photocatalytic reactor was irradiated with a visible light source radiating from a high-pressure 250 W Hg vapor lamp. In these experiments, 5 mL of the irradiated MB solution was withdrawn periodically, centrifuged to separate the catalyst and the absorbance of the supernatant dye solution was determined with the help of a UV–visible spectrometer at 664 nm. The percentage degradation of dye was calculated as per Eq. (1).

$$\%\ \text{Degradation} = [(C_o\text{-}C)/C_o] \times 100 \quad (1)$$

where, C_o is the initial concentration of dye solution and C is the concentration at different intervals of time.

To assess the major reactive species which are responsible for the photocatalytic degradation, trapping experiments were carried out by adding benzoquinone (1 mM), potassium iodide (10 mM), and isopropyl alcohol (10 mM) as scavengers for superoxide anion radicals ($O_2^{\cdot-}$), holes (h^+) and hydroxyl radicals (OH^-), respectively by following the similar procedure as that of the photocatalytic activity experiments.

3. Results and discussion

3.1. XRD, Raman and XPS analysis

The XRD patterns of the pure $CaTiO_3$ and the PGC composites with varying concentrations of PG shown in Fig. 1 could be indexed to the

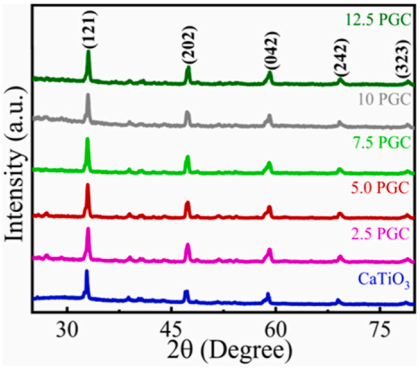

Fig. 1. XRD patterns of $CaTiO_3$ and PGC samples.

orthorhombic phase of $CaTiO_3$ with JCPDS card number 42–0423 [14]. A small shift in the diffraction angle of (121) plane from 32.83° ($CaTiO_3$) to 32.89° (7.5 PGC) indicates a conceivable interaction between the $CaTiO_3$ and the PG sheets in the composite (Fig. S1). The average crystallite sizes of the synthesized samples were calculated by using the values of diffraction angles and FWHM of (121) plane with the help of the Scherrer equation and the values were found to be 36.5 nm, 29.7 nm, 29.4 nm, 29.0 nm, 28.9 nm and 28.1 nm for $CaTiO_3$, 2.5 PGC, 5.0 PGC, 7.5 PGC, 10 PGC, and 12.5 PGC, respectively [30]. Since, no typical diffraction peaks for PG were observed in the composite materials due to the trace amount of PG with low atomic number which cannot be detected by the diffractometer used, Raman analysis was carried out to confirm the presence of PG [31].

Raman analysis of PG reveals a peak at 1347.2 cm^{-1} (D band), which could be assigned to the breathing mode of A_{1g} symmetry of the phonons near the K point and another peak at 1596.2 cm^{-1} (G band), which could be ascribed to the in-plane vibration of carbon atoms in sp^2 hybridized states (Fig. 2) [24,27]. Notably, in the case of the 7.5 PGC sample these peaks shift to 1350.2 cm^{-1} and 1593.2 cm^{-1}, due to the possible chemical interaction between the $CaTiO_3$ and the PG sheets. The degree of defects was derived from the intensity ratio of the D band to the G band (i.e. I_D/I_G) [32]. The I_D/I_G value in the case of 7.5 PGC (0.91) is lower than that of PG (1.07) due to the successful incorporation of $CaTiO_3$ cuboids on PG sheets [27,31,33].

The XPS survey spectrum of 7.5 PGC indicated the presence of Ca, Ti, O, and C in the composite (Fig. S2). The binding energy values of various elements in the high-resolution XPS spectra of 7.5 PGC indicated the presence of Ca in + 2 state, Ti in + 4 state (Fig. 3 and Table 1) [27, 33–39]. The existence of chemical interaction between $CaTiO_3$ and PG is indicated by the Ti-O-C bond formed which helps in the effective transfer of carriers from $CaTiO_3$ to PG thus increasing the separation of charge carriers, avoiding recombination of electrons and holes which in turn improves the photocatalytic efficiency [40,41].

3.2. Morphology and surface area analysis

The morphology of PG, $CaTiO_3$, and 7.5 PGC samples was investigated using FESEM and TEM analysis. $CaTiO_3$ particles exhibited a cuboidal shape while PG revealed wrinkled nature with many pores (Fig. 4 and Fig. S3). The TEM image of 7.5 PGC indicated $CaTiO_3$ cuboids partially wrapped in PG which promoted smooth migration of charge carriers [16,27]. Nitrogen adsorption-desorption isotherm of the 7.5 PGC can be classified as type IV with hysteresis loop H3 which is a characteristic of mesoporous materials (Fig. 5) [42]. The BET specific surface area of 7.5 PGC was found to be 31.9 $m^2\ g^{-1}$, which is higher than that of $CaTiO_3$ (15.9 $m^2\ g^{-1}$). This relatively higher surface area of the composite is due to the porous structure of PG which has an extremely high surface area [16]. The pore size distribution of the 7.5 PGC was analyzed by BJH analysis which revealed the mesoporous nature of the sample. The pore volume of 0.09 $cm^3\ g^{-1}$ of 7.5 PGC was also found to be higher than that of pure $CaTiO_3$ (0.02 $cm^3\ g^{-1}$). Relatively higher surface area and pore volume increases the photocatalytic activity due to enhanced adsorption of dye molecules on the surface for catalysis and rapid transport through the interlinking channels created by the pores [1,27,39].

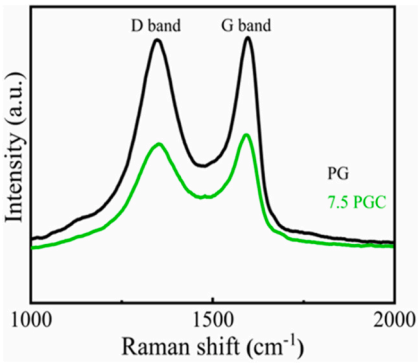

Fig. 2. Raman spectra of PG and 7.5 PGC.

3.3. Theoretical analysis

$CaTiO_3$ synthesized crystallized in orthorhombic structure and hence the same was used for the First principles density functional theory simulations. We see that the density of states (DOS) reveals an energy gap of 2.4 eV which is an underestimation compared to the experimental band gap of 3.2 eV reported previously (Fig. 6) [14]. Such kind of underestimation is well known in DFT based calculations [43]. Projection of atomic orbitals onto the DOS plot reveals that the conduction band is formed out of Ti 'p' states while the valence band is formed from O 'p' states similar to the case of other perovskite oxides like $SrTiO_3$ or $BaTiO_3$ [5,44]. Removal of a single carbon atom from graphene sheet to create a pore leads to opening up of zero band gap to 1.4 eV with a strong peak at the Fermi level created by the 's' and 'p' states of carbon atoms surrounding the pore [22,24]. The formation of PGC composite leads to formation of Ti-O-C bond by the overlap of 'd' states of Ti with 'p' states of O and C in the conduction band which leads to the easy migration of electrons promoted from the valence band of $CaTiO_3$ to its conduction band, to the PG thereby increasing the separation of charge carriers and increase in the lifetime of charge carriers.

3.4. Optical absorbance analysis

The optical absorption properties of the synthesized materials were investigated by DRS analysis (Fig. 7a). From the DR spectra, it can be seen that the absorption edges of PGC were shifted to the longer wavelength side as compared to $CaTiO_3$. The band gap of the synthesized catalysts was obtained using Tauc method where $(\alpha.h\nu)^{1/\gamma}$ was plotted against the band gap energy [1]. Here, α is the Kubelka-Munk function derived from Eq. (2).

$$\alpha = \frac{A}{S} = \frac{(1-R)^2}{2R} \tag{2}$$

where, R is the reflectance, A and S are the absorption and scattering coefficients, respectively [11]. The estimated band gaps were 3.27 eV, 3.14 eV, 2.94 eV, 2.78 eV, 2.62 eV and 2.51 eV for $CaTiO_3$, 2.5 PGC, 5.0 PGC, 7.5 PGC, 10 PGC and 12.5 PGC, respectively (Fig. S4).

Analysis of PL spectra has been widely used to investigate the lifetime of photoinduced charge carriers. From the PL spectra, a significant reduction in the fluorescence intensity of composite materials in comparison to $CaTiO_3$ was observed which was attributed to the efficient electron transport from $CaTiO_3$ to PG through the Ti-O-C bond thus enhancing the lifetime of photogenerated charge carriers by preventing electron hole recombination. However, beyond 7.5 PGC, the PL intensity was found to increase due to increase in recombination centers as a result of excess PG (Fig. 7b) [45].

3.5. Photocatalytic activity studies

During the photocatalytic study the percentage of MB removal by the $CaTiO_3$, 2.5 PGC, 5.0 PGC, 7.5 PGC, 10 PGC, and 12.5 PGC was found to be 14.0%, 74.0%, 88.0%, 98.1%, 90.0%, and 80.0%, respectively in 40 min (Fig. 8a). The duration of photocatalytic degradation of 7.5 PGC (40 min for 98.1%) was found to be much lower than that of N-$CaTiO_3$-rGO composite (180 min for 95%), $CaTiO_3$-gC_3N_4 (180 min for 30%) $SrTiO_3$-PG composite (120 min for 92%) and $BaTiO_3$-PG composite (80 min for 98.6%) reported earlier [16,25,27,46]. The performance is also found to be far better than other recently reported materials such as V doped $CaTiO_3$ (94.2% in 120 min), Eu and Na co-doped $CaTiO_3$

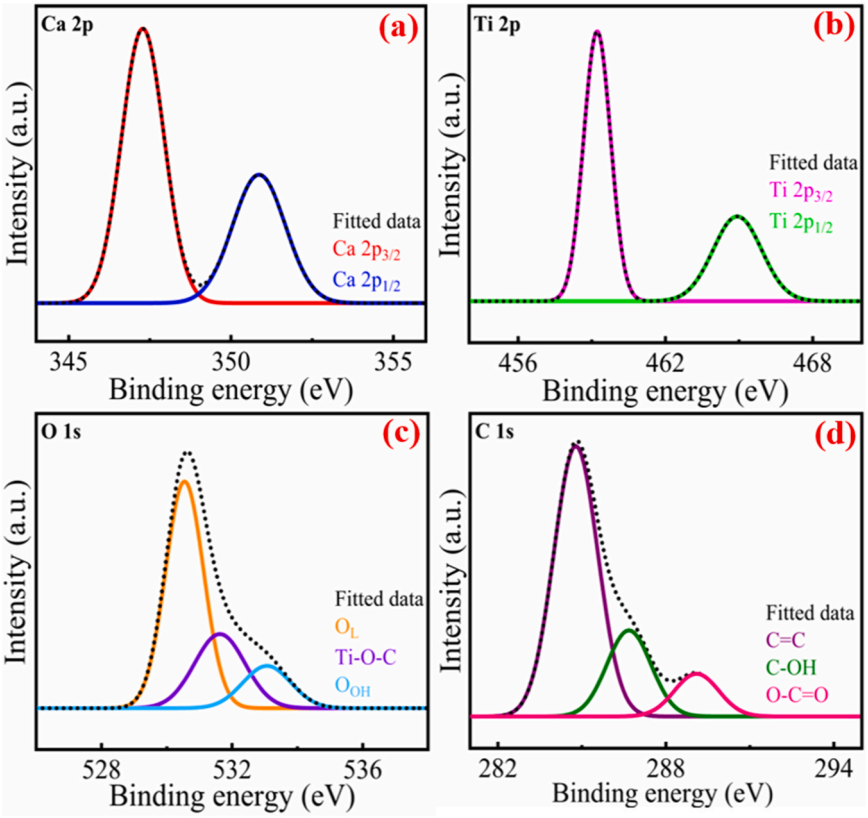

Fig. 3. High resolution XPS spectrum of 7.5 PGC (a) Ca 2p; (b) Ti 2p; (c) O 1 s; (d) C 1 s.

Table 1
XPS binding energy values of 7.5 PGC.

Element	Binding energy (eV)	Assignment	References
Ca 2p	347.3	Ca $2p_{3/2}$	31
	350.9	Ca $2p_{1/2}$	
Ti 2p	459.2	Ti $2p_{3/2}$	31,32
	464.9	Ti $2p_{1/2}$	
O 1 s	530.5	Lattice oxygen (O_L)	33-36
	533.1	Surface hydroxyl groups (O_{OH})	
	531.6	Ti-O-C	
C 1 s	284.7	C═C	26,30
	286.7	C-OH	
	289.1	O-C═O	

(96.62% in 300 min), Rh doped $BaTiO_3$ (96% in 120 min) and Cu doped $BaTiO_3$ (98.2% in 120 min) [14,17,37,39]. The outstanding photocatalytic efficiency of 7.5 PGC can be ascribed to the improved optical absorption ability in the visible region of the solar spectrum, relatively higher surface area which provides higher number of surface active sites for the efficient adsorption of MB, and efficacious interfacial charge transfer through the Ti-O-C bond which increases the lifetime of charge carriers. However, at higher concentrations of PG (i.e., beyond 7.5 wt %), the photocatalytic efficiency was found to be low due to the light-shielding effect caused by PG and also the formation of recombination centers as confirmed from the PL analysis.

To derive the kinetic information, the above photocatalytic degradation results were fitted with pseudo-first-order rate Eq. (3) [14,47].

$$\ln (C/C_o) = - kt \quad (3)$$

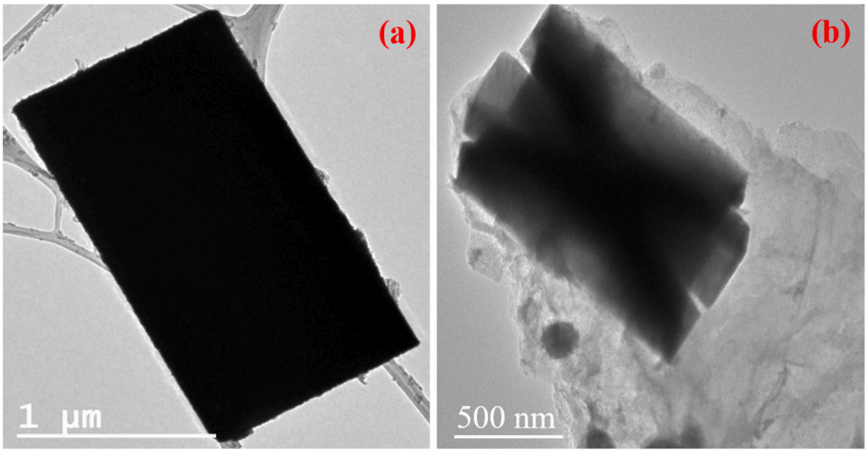

Fig. 4. TEM image of (a) $CaTiO_3$; (b) 7.5 PGC.

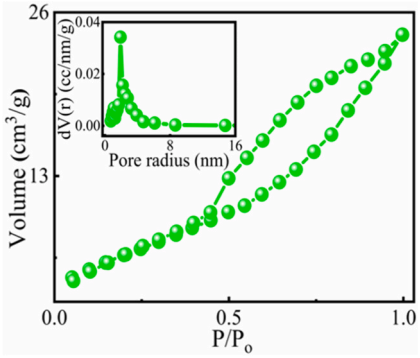

Fig. 5. Nitrogen adsorption-desorption isotherm of 7.5 PGC. Inset shows BJH pore size distribution.

where, 'C_o' is the initial concentration of the dye, 'C' is the concentration of the dye at irradiation time 't' and 'k' is the first-order rate constant which was determined from the slope of the linear fit of -ln (C/C_o) versus t [14,47]. Apparently, the rate constant of 7.5 PGC was found to be 0.0972 min^{-1}, which is far higher than that of pristine (0.0037 min^{-1}) (Fig. 8b). Cyclic stability is one of the important parameter to be considered for the practical application of catalyst. The slight deterioration in the photocatalytic activity of 7.5 PGC after seven successive cycles points towards its high stability (Fig. 8c). The TEM image of 7.5 PGC obtained after 7 cycles reveals slight crumpling of PG sheets which may have led to the minor deterioration in the photocatalytic activity (Fig. S5). The similar XRD patterns of the material before and after degradation of MB without generation of any additional peaks indicates that the crystal structure of the prepared compound is highly stable (Fig. S6).

Further, the radical scavenging experiments, indicated holes and hydroxyl radicals to be the main reactive species as the addition of corresponding scavenging agents efficiently suppressed the photocatalytic rate [48]. Further, superoxide anion radicals proved to be the less important reactive species as scavenging them did not affect the photocatalytic degradation of MB to a greater extent (Fig. 8d).

Based on this a mechanism was proposed for the degradation of MB as follows: Under visible light irradiation, an electron from the valence band gets excited to the conduction band of $CaTiO_3$ resulting in the

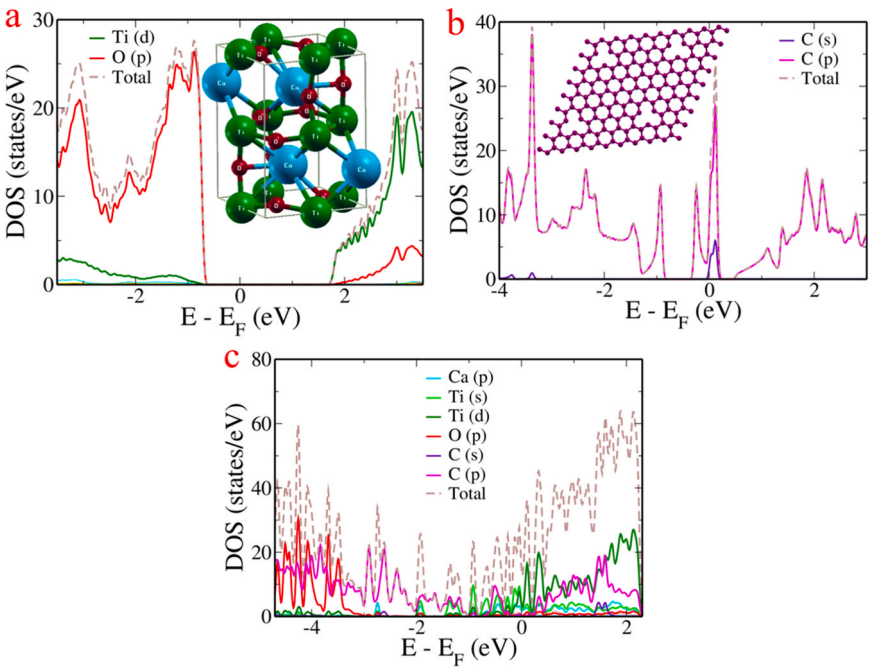

Fig. 6. pDOS of (a) $CaTiO_3$; (b) PG; (c) PGC. Inset shows crystal structure of orthorhombic $CaTiO_3$ and PG with single pore per 5 × 5 × 1 supercell dimension.

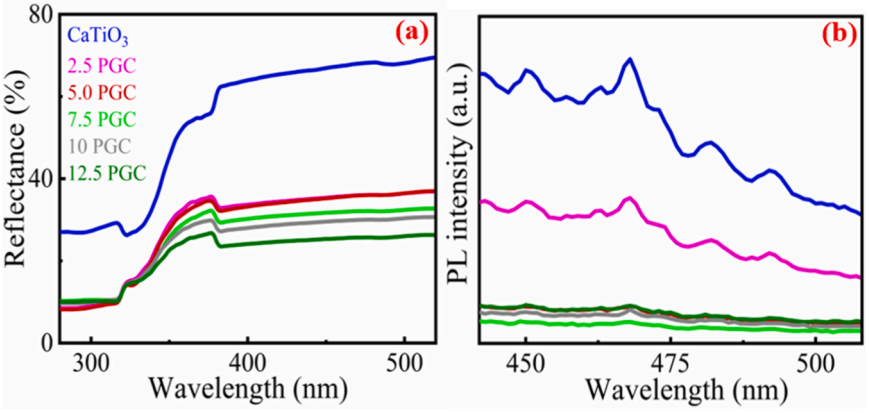

Fig. 7. (a) UV–visible DR spectra; (b) PL spectra of $CaTiO_3$ and PGC.

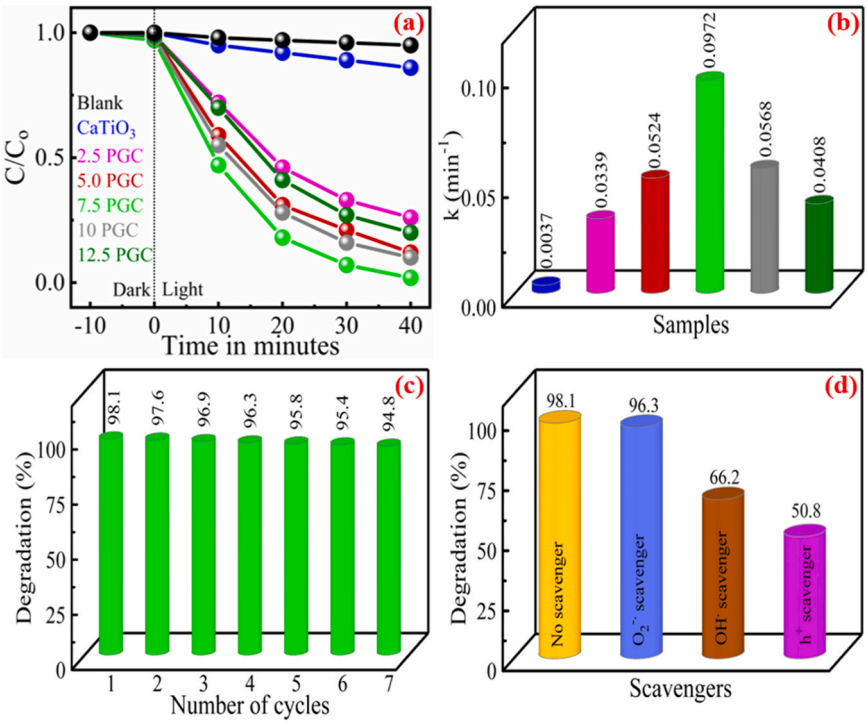

Fig. 8. (a) Photocatalytic degradation curves; (b) Rate constants of $CaTiO_3$ and PGC samples; (c) Cyclic stability plot of 7.5 PGC; (d) Effect of radical scavengers on the photocatalytic degradation of MB by 7.5 PGC.

formation of a hole in the valence band [14]. The electrons from the conduction band of $CaTiO_3$ transfer to the PG sheets through the Ti-O-C bonds. Owing to the excellent electronic conductivity of PG the charge carriers get separated thereby increasing the lifetime of photoinduced charge carriers (Fig. 9) [27]. These electrons further react with oxygen to generate superoxide anion radicals and moreover the holes directly oxidize MB or react with surface hydroxyl groups to generate hydroxyl radicals [49]. All these radicals react with MB dye molecules to produce simple products like CO_2, H_2O etc [50].

Activation complex theory and the Eyring equation were employed to determine various thermodynamic parameters [35,39]. From Table 2, we can observe that the activation energy (E_a) is higher for the photocatalytic degradation of MB without catalyst, whereas the energy of activation decreased in the presence of $CaTiO_3$ and PGC samples. This confirms that the catalyst provides an alternate path for the reaction with lower activation energy. 7.5 PGC revealed the relatively lower activation energy in comparison to other samples. The reaction's endothermic and non-spontaneous nature was confirmed by the positive enthalpy change ($\Delta H^{\#}$) and free energy change ($\Delta G^{\#}$) values [14,47].

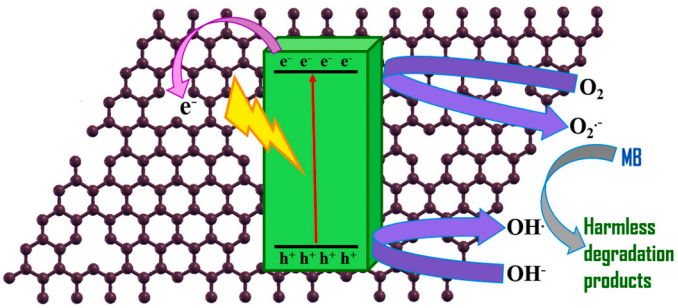

Fig. 9. Mechanism of photocatalytic degradation of MB by PGC.

Table 2
Thermodynamic parameters of $CaTiO_3$ and PGC samples for photodegradation of MB dye.

Sample	E_a (kJ/mol)	$\Delta H^{\#}$ (kJ/mol)	$\Delta S^{\#}$ (kJ/mol)	$\Delta G^{\#}$ (kJ/mol)
Without catalyst	16.6	14.1	-0.25	90.0
$CaTiO_3$	13.97	11.47	-0.25	87.44
2.5 PGC	8.44	5.94	-0.25	81.9
5.0 PGC	7.35	4.86	-0.25	80.82
7.5 PGC	5.81	3.32	-0.25	79.28
10 PGC	7.15	4.66	-0.25	80.62
12.5 PGC	7.98	5.48	-0.25	81.44

4. Conclusions

An excellent photocatalytic activity of 98.1% degradation of MB dye in 40 min was obtained by using porous graphene-$CaTiO_3$. This exceptional performance was a result of the decreased band gap of the composite which made it sensitive to visible light, the relatively higher surface area which helped in providing large number of active catalytic sites and the Ti-O-C bond formed which helped in the efficient separation of electron and hole pairs increasing the lifetime of charge carriers. Further, the enhanced cyclic and structural stability achieved along with high performance makes the solvothermal approach adopted an exceptional one which can be extended for the synthesis of other nanocomposites. The catalyst also shows promise to be studied for degradation of other pollutants.

Declaration of Competing Interest

The authors declare that they have no known competing financial interests or personal relationships that could have appeared to influence the work reported in this paper.

Data availability

Data will be made available on request.

Acknowledgement

The author USS acknowledges the financial support received from Science and Engineering Research Board, Government of India under SRS scheme.

Appendix A. Supporting information

Supplementary data associated with this article can be found in the online version at doi:10.1016/j.scenv.2024.100071.

References

1 Uma P.I, U.S. Shenoy, D.K. Bhat, Nanocubic Copper Doped $SrTiO_3$ for Photoreduction of Cr (VI) and Photodegradation of Methyl Violet, ACS Appl. Nano Mater. 6 (2023) 16798–16804.
2 M.M.J. Sadiq, U.S. Shenoy, D.K. Bhat, Synthesis of $BaWO_4$/NRGO–gC_3N_4 nanocomposites with excellent multifunctional catalytic performance via microwave approach, Front. Mater. Sci. 12 (2018) 247–263.
3 F. Mahmoudi, K. Saravanakumar, V. Maheskumar, L.K. Njaramba, Y. Yoon, C. M. Park, Application of Perovskite Oxides and Their Composites for Degrading Organic Pollutants from Wastewater Using Advanced Oxidation Processes: Review of the Recent Progress, J. Hazard. Mater. 436 (2022) 129074.
4 M. Li, N. Han, X. Zhang, S. Wang, M. Jiang, A. Bokhari, W. Zhang, M. Race, Z. Shen, R. Chen, M. Mubashir, Perovskite Oxide for Emerging Photo(electro)catalysis in Energy and Environment, Environ. Res. 205 (2022) 112544.
5 S.U. Shenoy, D.K. Bhat, Vanadium Doped $BaTiO_3$ as High Performance Thermoelectric Material: Role of Electronic Structure Engineering, Mat. Today Chem. 18 (2020) 100384.
6 S.U. Shenoy, D.K. Bhat, Enhanced Thermoelectric Properties of Vanadium Doped $SrTiO_3$: A Resonant Dopant Approach, J. Alloy. Compd. 832 (2020) 154958.
7 D.P. Jaihindh, B. Thirumalraj, S.M. Chen, P. Balasubramanian, Y.P. Fu, Facile Synthesis of Hierarchically Nanostructured Bismuth Vanadate: An Efficient Photocatalyst for Degradation and Detection of Hexavalent Chromium, J. Hazard. Mater. 367 (2019) 647–657.
8 H. Bantawal, U.S. Shenoy, D.K. Bhat, Tuning the Photocatalytic Activity of $SrTiO_3$ by Varying the Sr/Ti Ratio: Unusual Effect of Viscosity of the Synthesis Medium, J. Phys. Chem. C. 122 (2018) 20027–20033.
9 X. Zhang, X. Wang, J. Chai, S. Xue, R. Wang, L. Jiang, J. Wang, Z. Zhang, D. D. Dionysiou, Construction of Novel Symmetric Double Z-Scheme $BiFeO_3$/$CuBi_2O_4$/$BaTiO_3$ Photocatalyst with Enhanced Solar-Light-Driven Photocatalytic Performance for Degradation of Norfloxacin, Appl. Catal. B 272 (2020) 119017.
10 M.M.J. Sadiq, U.S. Shenoy, D.K. Bhat, Enhanced Photocatalytic Performance of N-Doped RGO-$FeWO_4$/Fe_3O_4 Ternary Nanocomposite in Environmental Applications, Mater. Today Chem. 4 (2017) 133–141.
11 P.I. Uma, S.U. Shenoy, D.K. Bhat, Electronic Structure Engineering of $BaTiO_3$ Cuboctahedrons by Doping Copper to Enhance the Photocatalytic Activity for Environmental Remediation, J. Alloy. Compd. 948 (2023) 169600.
12 J. Cai, A. Cao, J. Huang, W. Jin, J. Zhang, Z. Jiang, X. Li, Understanding Oxygen Vacancies in Disorder-Engineered Surface and Subsurface of $CaTiO_3$ Nanosheets on Photocatalytic Hydrogen Evolution, Appl. Catal. B 267 (2020) 118378.
13 E. Jiang, L. Yang, N. Song, X. Zhang, C. Liu, H. Dong, Multi-Shelled Hollow Cube $CaTiO_3$ Decorated with $Bi_{12}O_{17}Cl_2$ towards Enhancing Photocatalytic Performance Under the Visible Light, J. Colloid Interf. Sci. 576 (2020) 21–33.
14 H. Bantawal, U.S. Shenoy, D.K. Bhat, Vanadium doped $CaTiO_3$ cuboids: role of vanadium in improving the photocatalytic activity, Nanoscale Adv. 3 (2021) 5301–5311.
15 F. Dai, Y. Wang, R. Zhao, X. Zhou, J. Han, L. Wang, $ZnIn_2S_4$ Modified $CaTiO_3$ Nanocubes with Enhanced Photocatalytic Hydrogen Performance, Int. J. Hydrog. Energy 45 (2020) 28783–28791.
16 D.K. Bhat, H. Bantawal, P.I. Uma, U.S. Shenoy, Enhanced photoresponse and efficient charge transfer in porous graphene-$BaTiO_3$ nanocomposite for high performance photocatalysis, Diam. Relat. Mater. 139 (2023) 110312.
17 M. Chen, Q. Xiong, Z. Liu, K. Qiu, X. Xiao, Synthesis and Photocatalytic Activity of Na^+ Co-doped $CaTiO_3$: Eu^{3+} Photocatalysts for Methylene Blue Degradation, Ceram. Int. 46 (2020) 12111–12119.
18 M.M.J. Sadiq, U.S. Shenoy, D.K. Bhat, Novel RGO/$ZnWO_4$/Fe_3O_4 Nanocomposite as High Performance Visible Light Photocatalyst, RSC Adv. 6 (2016) 61821–61829.
19 T. Hisatomi, K. Domen, Reaction Systems for Solar Hydrogen Production via Water Splitting with Particulate Semiconductor Photocatalysts, Nat. Catal. 2 (2019) 387–399.
20 U.S. Shenoy, H. Bantawal, D.K. Bhat, Band Engineering of $SrTiO_3$: Effect of Synthetic Technique and Site Occupancy of Doped Rhodium, J. Phys. Chem. C. 122 (2018) 27567–27574.
21 M.M.J. Sadiq, U.S. Shenoy, D.K. Bhat, $NiWO_4$-ZnO-NRGO Ternary Nanocomposite as an Efficient Photocatalyst for Degradation of Methylene Blue and Reduction of 4-Nitro Phenol, J. Phys. Chem. Solids 109 (2017) 124–133.
22 M. Sethi, S.U. Shenoy, D.K. Bhat, Porous Graphene-$NiCo_2O_4$ Nanorod Hybrid Composite as High Performance Supercapacitor Electrode Material, N. J. Chem. 44 (2020) 4033–4041.
23 L. Wang, Z. Li, J. Chen, Y. Huang, H. Zhang, H. Qiu, Enhanced Photocatalytic Degradation of Methyl Orange by Porous Graphene/ZnO Nanocomposite, Environ. Pollut. 249 (2019) 801–811.
24 M. Sethi, H. Bantawal, U.S. Shenoy, D.K. Bhat, Eco-Friendly Synthesis of Porous Graphene and its Utilization as High Performance Supercapacitor Electrode Material, J. Alloy. Compd. 799 (2019) 256–266.
25 T. Xian, H. Yang, Y.S. Huo, Enhanced Photocatalytic Activity of $CaTiO_3$-Graphene Nanocomposites for Dye Degradation, Phys. Scr. 89 (2014) 115801.
26 A. Kumar, S. Kumar, A. Bahuguna, A. Kumar, V. Sharma, V. Krishnan, Recyclable, Bifunctional Composites of Perovskite Type N-$CaTiO_3$ and Reduced Graphene Oxide as an Efficient Adsorptive Photocatalyst for Environmental Remediation, Mater. Chem. Front. 1 (2017) 2391–2404.
27 H. Bantawal, M. Sethi, U.S. Shenoy, D.K. Bhat, Porous Graphene Wrapped $SrTiO_3$ Nanocomposite: Sr–C Bond as an Effective Coadjutant for High Performance Photocatalytic Degradation of Methylene Blue, ACS Appl. Nano Mater. 2 (2019) 6629–6636.
28 P. Giannozzi, S. Baroni, N. Bonini, M. Calandra, R. Car, C. Cavazzoni, D. Ceresoli, G. L. Chiarotti, M. Cococcioni, I. Dabo, et al., Quantum ESPRESSO: A Modular and Open-Source, Softw. Proj. Quantum Simul. Mater., *J. Phys.: Condens. Matter* 21 (2009) 395502.
29 J.P. Perdew, K. Burke, M. Ernzerhof, Generalized gradient approximation made simple, Phys. Rev. Lett. 77 (1996) 3865.
30 M. Sethi, U.S. Shenoy, D.K. Bhat, Hassle Free Solvothermal Synthesis of NiO Nanoflakes for Supercapacitor Application, Phys. B 611 (2021) 412959.
31 M.M.J. Sadiq, U.S. Shenoy, D.K. Bhat, Novel RGO–$ZnWO_4$–Fe_3O_4 Nanocomposite as High Performance Visible Light Photocatalyst, RSC Adv. 6 (2016) 61821–61829.
32 K. Wang, C. Miao, Y. Liu, L. Cai, W. Jones, J. Fan, D. Li, J. Feng, Vacancy Enriched Ultrathin TiMgAl-Layered Double Hydroxide/Graphene Oxides Composites as Highly Efficient Visible-Light Catalysts for CO_2 Reduction, Appl. Catal. B 270 (2020) 118878.
33 M. Sethi, U.S. Shenoy, D.K. Bhat, Simple Solvothermal Synthesis of Porous Graphene-NiO Nanocomposites with High Cyclic Stability for Supercapacitor Application, J. Alloy. Compd. 854 (2021) 157190.
34 Y. Yan, H. Yang, Z. Yi, R. Li, T. Xian, Design of Ternary $CaTiO_3$/g-C_3N_4/AgBr Z-Scheme Heterostructured Photocatalysts and their Application for Dye Photodegradation, Solid State Sci. 100 (2020) 106102.
35 H. Bantawal, U.S. Shenoy, D.K. Bhat, Vanadium-Doped $SrTiO_3$ Nanocubes: Insight into Role of Vanadium in Improving the Photocatalytic Activity, Appl. Surf. Sci. 513 (2020) 145858.
36 X. Shi, H. Yang, Z. Liang, A. Tian, X. Xue, Synthesis of Vertically Aligned $CaTiO_3$ Nanotubes with Simple Hydrothermal Method and its Photoelectrochemical Property, Nanotechnology 29 (2018) 385605.
37 P.I. Uma, S.U. Shenoy, D.K. Bhat, Doped $BaTiO_3$ Cuboctahedral Nanoparticles: Role of Copper in Photocatalytic Degradation of Dyes, *Appl. Surf. Sci. Adv.* 15 (2023) 100408.
38 X. Jiang, D. Yin, M. Yang, J. Du, W. Wang, L. Zhang, L. Yang, X. Han, B. Zhao, Revealing Interfacial Charge Transfer in TiO_2/Reduced Graphene Oxide Nanocomposite by Surface-Enhanced Raman Scattering (SERS): Simultaneous A Superior SERS-Active Substrate, Appl. Surf. Sci. 487 (2019) 938–944.
39 D.K. Bhat, H. Bantawal, U.S. Shenoy, Rhodium Doping Augments Photocatalytic Activity of Barium Titanate: Effect of Electronic Structure Engineering, Nanoscale Adv. 2 (2020) 5688–5698.
40 D.W. Boukhvalov, I.S. Zhidkov, A.I. Kukharenko, S.O. Cholakh, J.L. Menéndez, L. Fernández-García, E.Z. Kurmaev, Interaction of Graphene Oxide with Barium Titanate in Composite: XPS and DFT Studies, J. Alloy. Compd. 840 (2020) 155747.
41 C. He, X. Bu, S. Yang, P. He, G. Ding, X. Xie, Core-Shell $SrTiO_3$/Graphene Structure by Chemical Vapor Deposition for Enhanced Photocatalytic Performance, Appl. Surf. Sci. 436 (2018) 373–381.
42 M. Sethi, U.S. Shenoy, D.K. Bhat, A Porous Graphene–$NiFe_2O_4$ Nanocomposite with High Electrochemical Performance and High Cycling Stability for Energy Storage Applications, Nanoscale Adv. 2 (2020) 4229–4241.
43 S.U. Shenoy, D.K. Bhat, Electronic Structure Modulation of $Pb_{0.6}Sn_{0.4}Te$ via Zinc Doping and Its Effect on the Thermoelectric Properties, J. Alloy. Compd. 872 (2021) 159681.
44 S.U. Shenoy, D.K. Bhat, Electronic Structure Engineering of $SrTiO_3$ via Rhodium Doping: A DFT Study, J. Phys. Chem. Solids 148 (2021) 109708.
45 X. Liu, H. Ji, S. Li, W. Liu, Graphene modified anatase/titanate nanosheets with enhanced photocatalytic activity for efficient degradation of sulfamethazine under simulated solar light, Chemosphere 233 (2019) 198–206.
46 H. Shimamura, T. Nakamoto, K. Taguchi, Methylene Blue Decomposition in Visible Light by $CaTiO_3$/g-C_3N_4 Nanorods Produced by the Methanol Mixing Method, Energy Rep. 9 (2023) 284–287.
47 D.K. Bhat, P.I. Uma, U.S. Shenoy, Insights into the Dopant Engineering in Copper-Doped $SrTiO_3$ Nanocubes, *J. Hazard. Mater. Adv.* 12 (2023) 100380.
48 C.L. Ucker, S.R. Almedia, R.G. Cantoneiro, L.O. Diehl, S. Cava, M.L. Moreira, E. Longo, C.W. Raubach, Study of $CaTiO_3$-ZnS Heterostructure Obtained by

Microwave-Assisted Solvothermal Synthesis and its Application in Photocatalysis, J. Phys. Chem. Solids 172 (2023) 111050.
49 M.M.J. Sadiq, S.U. Shenoy, D.K. Bhat, Novel NRGO-$CoWO_4$-Fe_2O_3 Nanocomposite as an Efficient Catalyst for Dye Degradation and Reduction of 4-Nitrophenol, Mater. Chem. Phys. 208 (2018) 112–122.
50 J. Zhao, X. Cao, Y. Bai, J. Chen, C. Zhang, Simple Synthesis of $CaTiO_3$/g-C_3N_4 Heterojunction for Efficient Photodegradation of Methylene Blue and Levofloxacin, Opt. Mater. 135 (2023) 113239.